A Versatile Analytical Expression for the Inverse Abel Transform Applied to Experimental Data with Noise

SHUILIANG MA,* HONGMING GAO, GUANGJUN ZHANG, and LIN WU

State Key Laboratory of Advanced Welding Production Technology, Harbin Institute of Technology, Harbin 150001, China

A method for reconstruction of radially distributed plasma emission coefficients from projections with noise is proposed. The method represents the projections based on overlapping piecewise polynomial least squares fitting to take the inversion. Parameters that affect the inversion accuracy are analyzed and discussed in detail. Results for profiles with various shapes are presented and compared with those obtained with other methods. It is shown that for data with different numbers of points and different levels of noise, our method is more accurate and yields markedly better results for very sparse data. In addition, excellent results have been obtained from experimental intensities of an arc plasma without filtering of noise.

Index Headings: **Abel inversion; Arc plasma; Emission spectroscopy.**

INTRODUCTION

Thermal plasmas have been extensively used in many industrial fields, such as cutting, welding, spraying, surface modification, synthesis of fine powders, and waste treatment.[1,2] In order to improve and optimize the characteristics of these plasmas for their applications, one needs to have a good understanding of the behavior under different experimental conditions. The spatial distributions of plasma parameters, such as the electron density and temperature, could provide important insight into the basic processes that occur in the plasma. Therefore, spatially resolved measurements of these parameters are quite necessary and indispensable. Since such parameters in most circumstances are not uniformly distributed within the discharge, the collected intensity in spectroscopic measurements that is the projection of emission coefficients integrated along a chord in the plasma column cross-section should be converted to the original radial distribution (see Fig. 1). For cylindrically symmetric and optically thin plasmas, this can be implemented by using a method known as Abel inversion.[3]

Over the past years, a large number of methods have been developed for the inversion. Some methods are based on the polynomial interpolation technique,[4,5] which is a commonly used approach for function approximation. Because the influence of noise is not considered in these inversions, uncertainties in experimental data are greatly magnified due to the differential operator in the inverse Abel integral equation. Though it is possible to apply a smoothing process[6] before the inversion, in most cases the smoothing degree is very difficult to control. Algorithms using Fourier transform techniques[7,8] are also sensitive to noise, and the Fourier–Hankel method[9,10] cannot yield reasonable results for small sets of data, as demonstrated in Ref. 11. Methods employing spline techniques[12–14] were reported to be superior to other methods, with a high stability for resisting of noise, but when the noise is to be a magnitude larger, the methods are no longer suitable for use, and the poor inversion accuracy for off-axis peak profiles with very sparse data will lead to unacceptable results.[15] The only appropriate methods seem to be those using polynomial least squares techniques to fit the experimental data either in the whole segment[16,17] or in several divided ones.[18,19] Among them the method that breaks the whole interval into five segments[19] is more effective for yielding the best result in most situations. However, the larger errors near both ends of each segment fitted greatly deteriorate the inverted result. For these methods a common problem is that the inversion accuracy is very poor for small sets of data. In our experiments, the data collected with an optical fiber of a spectrograph are very limited; usually the number of points is from 20 to 50. The noise in the measured data evidently affects the inverted result when using methods such as that of Nestor and Olsen;[4] thus, it would be highly desirable to provide an appropriate method that is suitable for this case. In such a way, the noise in the experimental data does not need to be filtered or can be just partly filtered, and the result obtained is relatively good even for data with a very limited number of points.

This paper proposes a versatile Abel inversion method based on overlapping piecewise polynomial least squares fitting, which has a rather simple analytical expression but is very accurate even for very sparse data. In different cases, due to the smoothing property of the polynomial least squares fitting and the use of the segments overlapping technique, highly accurate results can be obtained by only adjusting one parameter according to the level of noise in the data. In the following sections we first describe the inversion method, then analyze the influences of different parameters and optimize their combinations, and at last show results obtained for simulated profiles and experimental data.

INVERSION METHOD

The forward Abel transform may be written as

$$I(y) = 2\int_y^1 \frac{\varepsilon(r)r}{\sqrt{r^2 - y^2}}\,\mathrm{d}r \tag{1}$$

where $I(y)$ represents the measured intensity and $\varepsilon(r)$ is the emission coefficient of the radiation source with a radius of unity. The inverse Abel transform for reconstruction of the emission coefficient is given by

$$\varepsilon(r) = \frac{1}{\pi}\int_r^1 \frac{I'(y)}{\sqrt{y^2 - r^2}}\,\mathrm{d}y \tag{2}$$

where $I'(y) = \mathrm{d}I(y)/\mathrm{d}y$.

In practice, however, there are two difficulties in applying Eq. 2 directly to experimental intensities. Values of the intensity measured are always in sets of discrete data, while a smooth function of $I(y)$ is required for calculating the integral.

Received 3 December 2007; accepted 27 March 2008.

* Author to whom correspondence should be sent. E-mail: shlgma@126.com.

0003-7028/08/6206-0701$2.00/0

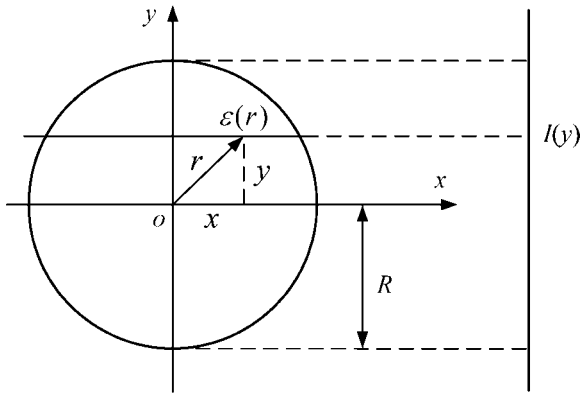

FIG. 1. Schematic diagram showing the coordinate system and geometry of a cylindrically symmetric radiation source with respect to the z-axis, which is normal to the paper.

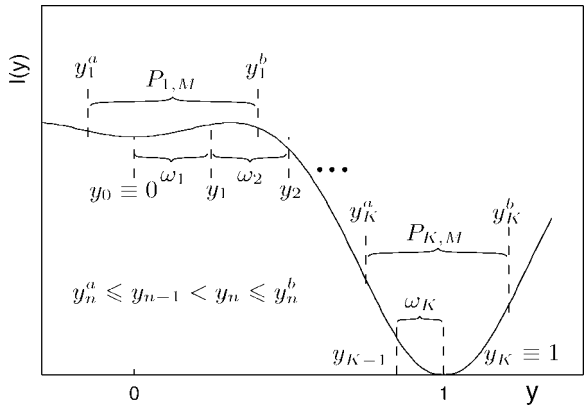

FIG. 2. Schematic representation of the overlapping piecewise polynomial least squares approximation for the intensity curve $I(y)$. $P_{n,M}$ denotes the polynomial of degree M fitted over segment $[y_n^a, y_n^b]$, and ω_n is the function for determining the segment $[y_{n-1}, y_n]$ for inversion.

Moreover, the random errors inherent in the measured data will be greatly magnified by the inverse transform, which involves numerical differentiation.

In this paper, both of the problems are resolved by representing the intensity profile with overlapping piecewise polynomials. Assume $I(y)$ is symmetric around $y = 0$, smooth and continuous as one period of a periodic function in the interval $[-1, 1]$; it can be approximated as

$$I(y) \simeq \sum_{n=1}^{K} \omega_n(y) P_{n,M}(y) = \sum_{n=1}^{K} \omega_n(y) \sum_{m=0}^{M} a_{n,m} y^m \quad (3)$$

where $\omega_n(y) = 1$ for $y_{n-1} \leq y \leq y_n$ and $\omega_n(y) = 0$ otherwise, and $P_{n,M}(y)$ is a polynomial of degree M defined over $[y_n^a, y_n^b]$, as shown in Fig. 2. Substituting Eq. 3 into Eq. 2 and with some simplifications, we have

$$\varepsilon_k(r) = -\frac{1}{\pi} \sum_{n=k}^{K} \sum_{m=1}^{M} m a_{n,m} [\delta_{n,k} I_{m-1}(r, y_n) + (1 - \delta_{n,k}) I_{m-1}(y_{n-1}, y_n)], \quad y_{k-1} \leq r \leq y_k \quad (4)$$

where $1 \leq k \leq K$, $\varepsilon_k(r)$ is the expression of the emission coefficient for the kth segment, δ is the Kronecker δ-function, and

$$I_m(a, b) = \int_a^b \frac{y^m}{\sqrt{y^2 - r^2}} \mathrm{d}y \quad (5)$$

Orthogonal polynomials have good properties for function least squares fitting.[16] With $f_{n,l}(y)$ as orthogonal polynomial basis functions,[20] $P_{n,M}(y)$ can be expanded as

$$P_{n,M}(y) = \sum_{l=0}^{M} c_{n,l} f_{n,l}(y) = \sum_{l=0}^{M} \sum_{m=0}^{l} c_{n,l} d_{n,l,m} y^m \quad (6)$$

where

$$c_{n,l} = \int_{y_n^a}^{y_n^b} f_{n,l}(y) I(y) \, \mathrm{d}y \quad (7)$$

and $d_{n,l,m}$ is the coefficient of y^m in $f_{n,l}(y)$, which is defined as

$$f_{n,l}(y) = \sqrt{\frac{2l+1}{y_n^b - y_n^a}} P_l\left(\frac{2y - y_n^b - y_n^a}{y_n^b - y_n^a}\right) \quad (8)$$

where $P_l(x)$ is the Legendre polynomial[21] of degree l defined over $[-1, 1]$. Taking an exchange in the order of the summation in Eq. 6 and comparing with Eq. 3, one obtains

$$a_{n,m} = \sum_{l=m}^{M} c_{n,l} d_{n,l,m} \quad (9)$$

Note that $c_{n,l}$ cannot be directly calculated using Eq. 7. Since $I(y)$ is assumed to be a periodic function, intensity data can be substituted by cubic interpolation functions. Under this condition, there is no difficulty to calculate the values of $c_{n,l}$. Therefore, using Eqs. 4, 5, and 9, the emission coefficient can be inverted readily. Also note that almost in all cases we force $I(y)$ to have a zero slope at the center, i.e., $I'(0) = 0$, which is desired for a cylindrically symmetric distribution. For Eq. 3 the condition can be satisfied only by setting $y_1^a = -y_1^b$. According to the arrangement of segments, the performance of the method can be very different. It is easy to see that the technique of Bockasten[5] and those fitting the intensity data to one curve[16,17] are two extremities of the method presented here. On the other hand, the algorithm of Cremers and Birkebak[19] is a compromise of the two kinds of methods. It is clear that if the combination of the parameters in Eq. 3 is optimized, the best performance can be achieved. This, as the main aim of this paper, is discussed in detail and presented in the following section.

RESULTS AND DISCUSSION

Test Profiles and Methods. It is always desirable to test a numerical method using simulated data, as the exact inversion is known and making a comparison between results obtained with different methods is possible. For this purpose, a total of four test profiles of two types are chosen from numerical examples in the literature.[14,19,22,23] Figure 3 shows the radial emission coefficient distributions of these profiles. Two of them are for the usual bell-shaped distributions. They are given by

$$\varepsilon_1(r) = (1 - r)^2 (1 + 2r), \quad 0 \leq r \leq 1 \quad (10)$$

and

$$\varepsilon_2(r) = \begin{cases} 1 - 2r^2, & 0 \leq r \leq 0.5 \\ 2(1 - r^2), & 0.5 < r \leq 1 \end{cases} \quad (11)$$

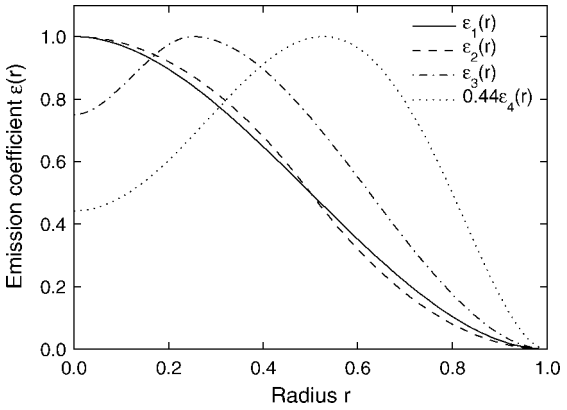

FIG. 3. Radial distributions of the emission coefficient of four test profiles.

The other two are for the off-axis peak type of distributions, which are expressed as

$$\varepsilon_3(r) = \begin{cases} \frac{3}{4} + 12r^2 - 32r^3, & 0 \le r \le 0.25 \\ \frac{16}{27}(1-r)^2(1+8r), & 0.25 < r \le 1 \end{cases} \tag{12}$$

and

$$\varepsilon_4(r) = (1-r^2)^2(1+12r), \qquad 0 \le r \le 1 \tag{13}$$

Both of the two types are commonly encountered in plasma diagnostics. In our experiment for a dc argon arc, the bell-shaped distributions typically appear in the anode arc column, and the off-axis peak profiles are characteristic distributions of the cathode arc column with high temperatures.

Intensity data are needed as the input of inversion; thus, the corresponding values of $I_1(y)$ to $I_4(y)$ are obtained by direct integration of Eq. 1. As demonstrated in many studies,[14,19] the off-axis peak distribution is much more difficult to reconstruct faithfully than other types with simple shapes such as $\varepsilon_1(r)$ and $\varepsilon_2(r)$. Therefore, we use I_4 to investigate the effect of different parameters on the accuracy of the new method, then use I_1 through I_3 to validate the possibility with the optimized parameters for inversion of profiles with different shapes and make a comparison with other methods.

The experimentally measured data in practice are unavoidably distorted by noise. To test the properties of the method for input values with errors, the data of I_1 through I_4 were rounded off to two decimal places or included different levels of normally distributed random noise with an absolute scale independent of the test profiles to simulate experimental uncertainties.

To estimate the performance of the method with different parameters and compare the results with those obtained using other methods, we calculated the absolute inversion error at each point:

$$\Delta\varepsilon(r_i) = \varepsilon_t(r_i) - \varepsilon_c(r_i) \tag{14}$$

where $\varepsilon_t(r_i)$ is the theoretical emission coefficient at point r_i, and $\varepsilon_c(r_i)$ is the calculated value at the corresponding point, and we also calculated the standard deviation σ, defined by

$$\sigma = \left\{ \frac{1}{N} \sum_{i=1}^{N} [\varepsilon_t(r_i) - \varepsilon_c(r_i)]^2 \right\}^{1/2} \tag{15}$$

Influence of Different Parameters. As can be seen from Eq. 3, in order to achieve the best performance with the proposed method several parameters should be optimized, such as the arrangement of the segments for both approximation and inversion and the degree of polynomial used for least squares fitting. For simplicity, all the segments were set to an equal length, i.e., $y_n - y_{n-1}$ are the same for all values of n, except $n = K$, for which the length of the last segment may be equal to or less than those of other ones. Though the degree of the polynomial used for each segment can be different, here only the case in which all segments employ polynomials with the same degree will be explored. Considering the inability of using polynomials with too low degrees for approximation and the difficulty of suppressing noise using polynomials with too high degrees, the values of M were chosen as 4, 6, and 8.

The first parameter that should be optimized is the length of the segment for approximation, which determines the overlapping amount of two near segments (see Fig. 2). It is defined as the overlapping factor

$$\rho = (y_n^b - y_n^a)/R \tag{16}$$

where R is the radius of the source, which is normalized to unity in this paper.

There are two advantages to the near segments being overlapped. The larger fitting errors invariably encountered near the ends of the data interval (this is the so-called termination error)[24] are avoided under this condition as both end parts of each fitted profile are dropped with the overlapping technique, so the inverted curve will be more smooth and accurate. Also, since the segment for approximation has a longer length than that for inversion, more data points have been used for approximation, and thus fitted accuracy can be improved, especially for small sets of data with noise. As can be found from the example presented below that the inversion error indeed decreased with the increase of the overlapping factor.

To optimize the overlapping factor ρ, random noise with a standard deviation $S = 0.01$ was added to the values of I_4 before taking the inversion. Results obtained with various values of ρ are shown in Fig. 4. As expected, the inversion accuracy keeps improving with the increase of ρ. The standard deviation σ bottomed out at certain positions for different values of M. A detailed study indicates that for large values of ρ, the approximated function for each segment failed to accurately represent the intensity profile, and thus σ increases as ρ tends to 1. The increasing trend is most significant for $M = 4$, since a polynomial with a lower degree is more difficult to fit to the real distribution of data. Therefore, the value of ρ should be chosen between $1/K$ and 0.7, 0.8, and 0.9 for $M = 4$, 6, and 8, respectively, depending on the level of noise in the data to be inverted. For experimental data with weak noise, the value of ρ can be lowered appropriately.

Then the effect of the number of segments on the inversion accuracy is analyzed using two sets of data with $N = 100$. One was used as the input value of the presented method with a low level of noise of $S = 0.005$, and the other included a high level of noise with $S = 0.05$. The overlapping factors for polynomials with degrees $M = 4$, 6, and 8 were set as 0.4, 0.5, and 0.6 for $S = 0.005$, and 0.5, 0.7, and 0.8 for $S = 0.05$. The calculated standard deviations are shown in Figs. 5a and 5b, respectively. It is clear that the influence of the number of segments is not significant. With the increase of K, σ increases very slowly. For $K \le 5$ the inversion error is relatively small. However,

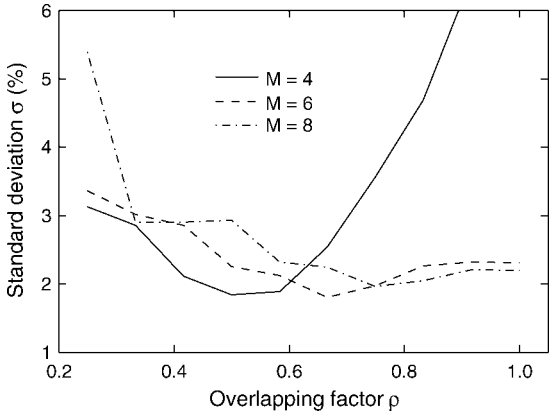

FIG. 4. Standard deviations calculated with $K = 4$ and various values of ρ for I_4 with $N = 24$ and $S = 0.01$.

there is one exception; for $K = 2$, big errors appeared for the inversion with $M = 4$, which once again indicates the limited ability for fitting profiles faithfully using polynomials with $M \leq 4$. Therefore, for practical utilization we recommend that the value of K should be no less than 3, although for $K = 2$ values of σ obtained with $M = 6$ and 8 are much smaller. Considering that the use of a large number of segments cannot improve inversion accuracy but increases computational time, the value of K should be chosen between 3 and 5.

The inversion accuracy will also depend on the number of

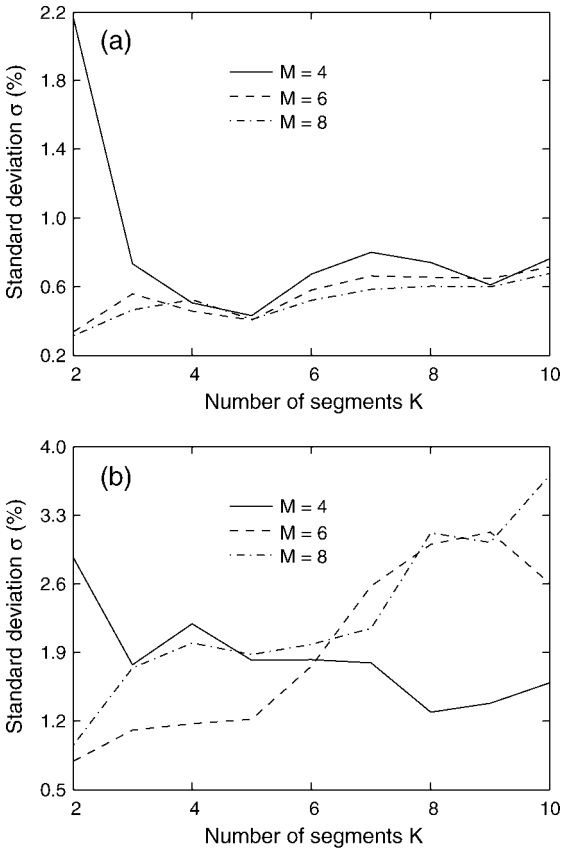

FIG. 5. Standard deviations calculated with various values of K for I_4 with $N = 100$, (**a**) $S = 0.005$, ρ = 0.4, 0.5, and 0.6; and (**b**) $S = 0.05$, ρ = 0.5, 0.7, and 0.8 for $M = 4$, 6, and 8, respectively.

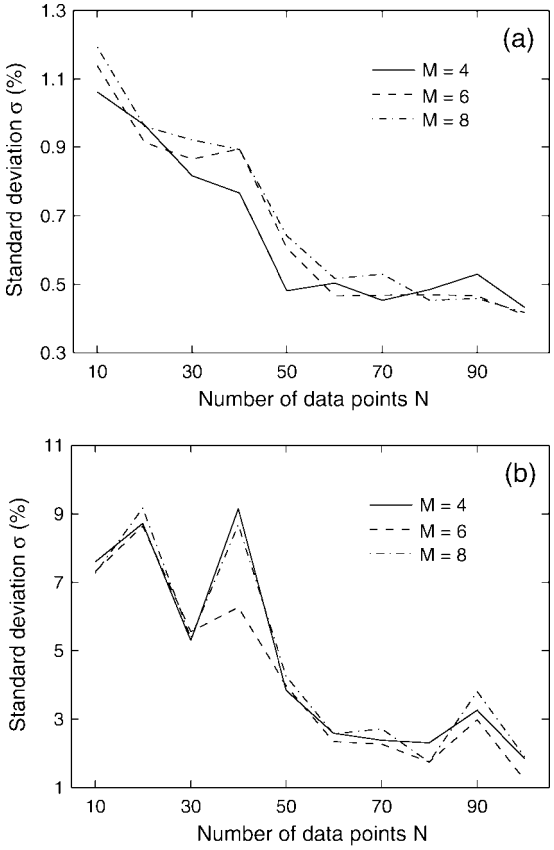

FIG. 6. Standard deviations calculated with $K = 5$ and various values of N for I_4 with (**a**) $S = 0.005$, and (**b**) $S = 0.05$. Other conditions are the same as Fig. 5.

data points. To find this relation, two series of data sets the same as those used in Figs. 5a and 5b but with different values of N were generated. The results inverted with $K = 5$ are shown in Figs. 6a and 6b. Since the value of the number of segments was chosen appropriately, there is no significant difference between the results inverted with $M = 4$, 6, and 8. With the increase of N, σ indeed decreased. But for $N \geq 50$ the improvement becomes minimal for the data with either a low or high level of noise. Therefore, when $N < 50$, it is better to use techniques such as interpolation to improve the inversion accuracy. On the other hand, when $N \geq 50$, there is no need to increase the number of data points before inversion.

Comparison with Other Algorithms. According to the results of the previous section, we used the method to take an inversion with $K = 5$, $M = 4$. We chose $M = 4$ because a good comparison with the Cremers and Birkebak method[19] is possible. In general, other parameters may be possible for achieving better results.

First, the method was applied to the data of I_3 with and without uncertainties. The absolute inversion errors obtained are listed in Table I. This illustrates the differences in the results between our method and that of Cremers and Birkebak. For accurate data, the result of Cremers and Birkebak is a little superior. For data rounded off to two decimal places, which is approximately equivalent to those including normally distributed random noise with a standard deviation, $S \approx 0.00289$; however, our method gives more accurate results. Since both the methods use the same number of segments and the same polynomial degree, the improvement is considered to be due to

TABLE I. Comparison of absolute inversion errors obtained for accurate data of I_3 and those rounded off to two decimal places with $N = 30$.

	$S = 0$		$S \approx 0.00289$	
i	Cremers and Birkebak, 4th deg	This work, $M = 4$, $\rho = 0.5$	Cremers and Birkebak, 4th deg	This work, $M = 4$, $\rho = 0.5$
0	-1.8×10^{-3}	2.1×10^{-4}	-3.9×10^{-2}	-2.1×10^{-2}
1	-3.0×10^{-4}	1.9×10^{-3}	-3.1×10^{-2}	-1.6×10^{-2}
2	1.2×10^{-3}	3.8×10^{-3}	-1.3×10^{-3}	-6.6×10^{-3}
3	1.2×10^{-3}	4.2×10^{-3}	4.3×10^{-3}	2.9×10^{-3}
4	0.0×10^{-4}	3.3×10^{-3}	1.2×10^{-2}	9.2×10^{-3}
5	-3.6×10^{-3}	2.9×10^{-3}	-1.4×10^{-3}	1.1×10^{-2}
6	3.5×10^{-3}	2.8×10^{-3}	5.0×10^{-3}	4.8×10^{-3}
7	7.3×10^{-3}	9.0×10^{-3}	8.4×10^{-3}	1.1×10^{-2}
8	2.9×10^{-3}	6.3×10^{-3}	4.0×10^{-3}	8.8×10^{-3}
9	-1.3×10^{-3}	2.3×10^{-3}	0.0×10^{-4}	4.7×10^{-3}
10	-2.9×10^{-3}	-5.2×10^{-4}	-1.5×10^{-3}	1.1×10^{-3}
11	1.0×10^{-4}	-1.7×10^{-3}	8.0×10^{-4}	-1.4×10^{-3}
12	3.0×10^{-4}	4.3×10^{-4}	-1.3×10^{-3}	-2.3×10^{-3}
13	4.0×10^{-4}	7.6×10^{-4}	-2.2×10^{-3}	-2.5×10^{-3}
14	3.0×10^{-4}	8.6×10^{-4}	-2.3×10^{-3}	-1.9×10^{-3}
15	2.0×10^{-4}	7.5×10^{-4}	-1.5×10^{-3}	-9.2×10^{-4}
16	0.0×10^{-4}	5.3×10^{-4}	2.0×10^{-4}	2.4×10^{-4}
17	0.0×10^{-4}	3.2×10^{-4}	4.5×10^{-3}	1.6×10^{-3}
18	3.0×10^{-4}	2.6×10^{-4}	4.6×10^{-3}	4.9×10^{-3}
19	4.0×10^{-4}	6.7×10^{-4}	3.0×10^{-3}	2.9×10^{-3}
20	3.0×10^{-4}	8.5×10^{-4}	6.0×10^{-4}	2.5×10^{-4}
21	2.0×10^{-4}	7.7×10^{-4}	-1.9×10^{-3}	-2.2×10^{-3}
22	0.0×10^{-4}	5.1×10^{-4}	-3.8×10^{-3}	-3.7×10^{-3}
23	1.0×10^{-4}	2.5×10^{-4}	-5.7×10^{-3}	-3.7×10^{-3}
24	4.0×10^{-4}	4.0×10^{-4}	-1.8×10^{-3}	-1.9×10^{-3}
25	4.0×10^{-4}	4.6×10^{-4}	2.7×10^{-3}	2.3×10^{-3}
26	1.0×10^{-4}	2.0×10^{-4}	4.6×10^{-3}	4.6×10^{-3}
27	-3.0×10^{-4}	-1.6×10^{-4}	4.6×10^{-3}	4.4×10^{-3}
28	-3.0×10^{-4}	-2.2×10^{-4}	2.5×10^{-3}	1.8×10^{-3}
29	4.0×10^{-4}	4.5×10^{-4}	-5.0×10^{-4}	-1.5×10^{-3}
30	0.0×10^{-0}	0.0×10^{-0}	0.0×10^{-0}	0.0×10^{-0}
σ	1.8×10^{-3}	2.5×10^{-3}	1.0×10^{-2}	6.6×10^{-3}

the use of the overlapping technique. It is interesting to notice that the superior method for accurate data now turns out to be the worst method when uncertainties are presented in the intensities.

Then, with our method for the first three test profiles I_1 to I_3 with and without error, using a varying number of data points, standard deviations of the inversion are obtained, as presented in Table II, where the results of the fourth degree method of Cremers and Birkebak and the spline interpolation method[14] are also listed for comparison. For data with $S = 0$, the results of our method are presented only to show the highest accuracy that can be achieved. By adjusting parameters such as the degree of the polynomial and the number of segments, more accurate result will be obtained, as shown in Ref. 18. Since experimental data that unavoidably have uncertainties cannot be measured with a high accuracy, results inverted for data with error will be more valuable. For data rounded off to two decimal places our method is superior to the other two methods, except for the case of I_3, for which the spline interpolation method yields more accurate results. In fact, rounding the profile of I_3 to two decimal places is not equivalent to adding normally distributed random noise as at the region near the center of the source the magnitude of I_3 varies very slow. Therefore, comparison for data with random noise will be more reliable.

Finally, we studied the performance of the method for data with different levels of random noise. The results obtained are listed in Table III. When $S < 0.1$, for I_2 the result of our method is still more accurate than that obtained with the Cremers and Birkebak and spline interpolation methods, and for I_3 the value of σ obtained with the spline interpolation method is about 3 to 10 times higher than ours for $N \leq 30$, and that of the Cremers and Birkebak method is also higher. Note that in contrast to the results shown in Table II, the spline interpolation method now becomes the worst for profile I_3 with random noise. When $S = 0.1$, results obtained with all three methods are unacceptable due to the high level of noise in the data, which is not very realistic in experiments. If such a case is encountered, a smoothing technique should be implemented before the inversion.

From these examples, it is evident that our method yields much better results than other methods for data either with different numbers of points or with different levels of noise; even for $N \leq 15$, our method is still very accurate, almost ten times as accurate as the spline interpolation method for the off-axis peak profile I_3.

Experimental Results. It would be of great interest to test the new method further with experimental data as all algorithms should ultimately be used in practice. The plasma intensities for the inversion were collected at several layers of a dc argon arc burning free at atmospheric pressure. The arc current was 200 A, and the distance from the cathode tip to the anode plate was 5 mm. Light from the arc was imaged at a magnification of 2:1 onto a plane parallel to the arc axis, where an optical fiber was moved by a motor across the axis in the horizontal direction. The light in the fiber was then collimated onto the entrance slit of a spectrograph and recorded with a charge-coupled device (CCD). In such a way, chordal

TABLE II. Standard deviations obtained for I_1 to I_3. Data for the spline interpolation method were taken from $g^c(r)$ in Ref. 14.

	$S = 0$			$S \approx 0.00289$		
N	Cremers and Birkebak, 4th deg	Spline interpolation	This work, $M = 4$, $\rho = 0.6$	Cremers and Birkebak, 4th deg	Spline interpolation	This work, $M = 4$, $\rho = 0.6$
I_1						
10	1.8×10^{-1}	1.3×10^{-3}	9.3×10^{-4}	1.8×10^{-1}	1.5×10^{-2}	3.7×10^{-3}
20	4.0×10^{-4}	6.8×10^{-4}	1.0×10^{-3}	6.7×10^{-3}	4.5×10^{-3}	9.1×10^{-3}
30	1.3×10^{-4}	1.9×10^{-4}	9.9×10^{-4}	3.7×10^{-3}	2.8×10^{-3}	2.3×10^{-3}
40	7.8×10^{-5}	4.2×10^{-5}	9.7×10^{-4}	6.0×10^{-3}	4.1×10^{-3}	3.0×10^{-3}
50	6.5×10^{-5}	4.3×10^{-5}	9.6×10^{-4}	5.7×10^{-3}	3.4×10^{-3}	1.9×10^{-3}
100		2.5×10^{-6}	9.2×10^{-4}		3.2×10^{-3}	1.3×10^{-3}
I_2						
10	1.8×10^{-1}	2.5×10^{-2}	1.9×10^{-3}	1.8×10^{-1}	2.4×10^{-2}	5.6×10^{-3}
20	1.5×10^{-3}	9.5×10^{-4}	2.4×10^{-3}	4.2×10^{-3}	5.0×10^{-3}	5.7×10^{-3}
30	9.2×10^{-4}	2.9×10^{-4}	2.3×10^{-3}	7.1×10^{-3}	7.0×10^{-3}	6.0×10^{-3}
40	7.6×10^{-4}	1.6×10^{-4}	2.3×10^{-3}	7.0×10^{-3}	5.3×10^{-3}	4.9×10^{-3}
50	7.0×10^{-4}	1.5×10^{-4}	2.3×10^{-3}	5.3×10^{-3}	3.2×10^{-3}	2.5×10^{-3}
100		2.7×10^{-5}	2.2×10^{-3}		5.7×10^{-3}	2.9×10^{-3}
I_3						
10	2.1×10^{-1}	1.2×10^{-1}	6.9×10^{-3}	2.1×10^{-1}	1.2×10^{-1}	1.4×10^{-2}
20	3.5×10^{-3}	3.5×10^{-3}	7.1×10^{-3}	1.0×10^{-2}	4.2×10^{-3}	8.8×10^{-3}
30	1.8×10^{-3}	2.4×10^{-3}	6.9×10^{-3}	1.0×10^{-2}	5.2×10^{-3}	8.0×10^{-3}
40	1.3×10^{-3}	4.1×10^{-4}	6.7×10^{-3}	9.9×10^{-3}	5.0×10^{-3}	8.4×10^{-3}
50	1.1×10^{-3}	3.8×10^{-4}	6.6×10^{-3}	1.1×10^{-2}	5.6×10^{-3}	7.9×10^{-3}
100		5.5×10^{-5}	6.4×10^{-3}			7.5×10^{-3}

projections from different layers of the arc were measured. Figure 7a shows the intensity distributions of the Ar I 696.5 nm line measured from layers of the arc with distances of 0.5, 1.5, 2.5, and 3.5 mm from the cathode tip; the number of data points for these profiles is 40, 50, 60, and 60, respectively.

No interpolation was used on the experimental data as the number of data points is large enough. For the inversion, we use $K = 5$, $M = 6$. The noise in the measured data was estimated to have a standard deviation of $S = 0.007$, and considering the long tails in the distributions of the intensity profiles, the overlapping factor was therefore determined as 0.35. The results inverted with the Nestor–Olsen method[4] and the algorithm presented in this paper are shown in Figs. 7b and 7c, respectively. It is evident that the distributions of the profiles in Fig. 7c are similar to those shown in Fig. 7b. This indicates that the original data were not distorted by the polynomial fitting technique, and thus the results obtained are reliable. The profiles inverted with our method are smooth and continuous; the noise in the original data is completely suppressed due to the excellent smoothing property of the polynomial least squares fitting technique. It must be noticed that the first three profiles are off-axis peak distributions and the last one belongs to the bell-shaped type. Good results obtained for these profiles again validate the ability of our method for successfully applying to experimental data with various shapes that are commonly encountered in plasma diagnostics.

TABLE III. Standard deviations obtained for I_2 and I_3 with different levels of noise. Data for the spline interpolation method were taken from Ref. 15. Data from this work were inverted with $\rho = 0.6$, 0.7, and 0.8 for $S = 0.005$, 0.01, and 0.1, respectively.

	I_2			I_3		
N	Cremers and Birkebak, 4th deg	Spline interpolation	This work, $M = 4$	Cremers and Birkebak, 4th deg	Spline interpolation	This work, $M = 4$
$S = 0.005$						
5	2.3×10^{-2}	4.0×10^{-2}	9.8×10^{-3}	2.1×10^{-2}	1.2×10^{-1}	1.4×10^{-2}
10	1.5×10^{-2}	2.2×10^{-2}	1.5×10^{-2}	1.7×10^{-2}	1.1×10^{-1}	1.8×10^{-2}
15	1.3×10^{-2}	6.7×10^{-3}	5.0×10^{-3}	1.5×10^{-2}	3.5×10^{-2}	6.0×10^{-3}
30	7.8×10^{-3}	5.6×10^{-3}	6.2×10^{-3}	7.9×10^{-3}	1.8×10^{-2}	7.1×10^{-3}
50	6.6×10^{-3}	3.9×10^{-3}	9.3×10^{-3}	6.7×10^{-3}	9.2×10^{-3}	9.5×10^{-3}
$S = 0.01$						
5	3.6×10^{-2}	4.5×10^{-2}	1.7×10^{-2}	2.9×10^{-2}	1.2×10^{-1}	2.1×10^{-2}
10	2.6×10^{-2}	2.3×10^{-2}	3.0×10^{-2}	2.8×10^{-2}	1.1×10^{-1}	3.2×10^{-2}
15	2.5×10^{-2}	2.3×10^{-2}	5.4×10^{-3}	2.7×10^{-2}	1.2×10^{-1}	8.4×10^{-3}
30	1.5×10^{-2}	1.1×10^{-2}	8.2×10^{-3}	1.5×10^{-2}	2.9×10^{-2}	9.7×10^{-3}
50	1.3×10^{-2}	7.4×10^{-3}	1.2×10^{-2}	1.3×10^{-2}	1.3×10^{-2}	1.2×10^{-2}
$S = 0.1$						
5	3.5×10^{-1}	5.2×10^{-2}	1.6×10^{-1}	3.4×10^{-1}	2.8×10^{-1}	1.6×10^{-1}
10	2.5×10^{-1}	1.0×10^{-1}	2.2×10^{-1}	2.5×10^{-1}	1.2×10^{-1}	2.2×10^{-1}
15	2.4×10^{-1}	9.3×10^{-2}	5.6×10^{-2}	2.4×10^{-1}	7.8×10^{-2}	5.4×10^{-2}
30	1.5×10^{-1}	5.2×10^{-3}	5.5×10^{-2}	1.5×10^{-1}	8.6×10^{-2}	5.2×10^{-2}
50	1.3×10^{-1}	6.2×10^{-2}	9.8×10^{-2}	1.3×10^{-1}	1.1×10^{-1}	1.0×10^{-1}

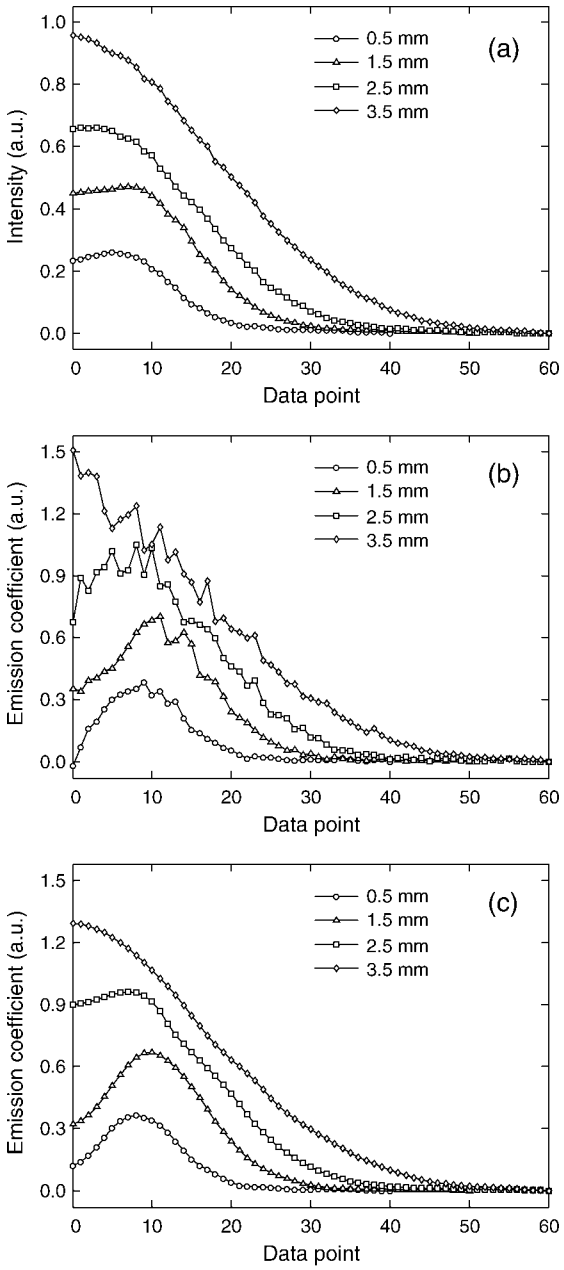

FIG. 7. Distributions of (**a**) experimental intensities measured from different layers of an arc plasma, and the corresponding radial emission coefficients inverted with (**b**) the Nestor–Olsen method and (**c**) the algorithm proposed in this paper with $K = 5$, $M = 6$, and $\rho = 0.35$.

CONCLUSION

A versatile analytical expression as well as its Abel inverse was presented for reconstruction of plasma emission coefficients from projected intensities with noise. The investigation with simulated data indicated that the method can suppress noise very effectively by using the optimized combination of parameters, and it is superior to other methods, such as those using the techniques of polynomial least squares fitting and spline interpolation, especially for data with a very limited number of points. Excellent results were obtained with the proposed method being applied to experimental data without removal of noise.

The good performance of the method is achieved due to the following aspects. First, polynomial least squares fitting greatly reduces the effect of noise, and thus a good inversion can be obtained even for data with experimental uncertainties. Second, dividing the interval of data measurement into several segments ensures that the measured profile is not distorted by the fitting process and at the same time improves the approximation accuracy; therefore, the method is possible for applying to profiles with various shapes with a high inversion accuracy. Lastly, the use of the overlapping segment technique not only avoids termination errors but also increases the number of data points for fitting, which leads to more accurate inversions even for small sets of data. Consequently, the method is more suitable than other ones for applying to experimental data, for which the noise filtering process is not required.

ACKNOWLEDGMENTS

This work is supported by the Chinese Natural Science Foundation under Contract No. 50775053. The comments of the anonymous reviewers are gratefully acknowledged.

1. P. Fauchais and A. Vardelle, IEEE Trans. Plasma Sci. **25,** 1258 (1997).
2. U. Kogelschatz, Plasma Phys. Control. Fusion **46,** B63 (2004).
3. H. R. Griem, *Principles of Plasma Spectroscopy* (Cambridge University Press, Cambridge, 1997).
4. O. H. Nestor and H. N. Olsen, SIAM Rev. **2,** 200 (1960).
5. K. Bockasten, J. Opt. Soc. Am. **51,** 943 (1961).
6. R. Álvarez, A. Rodero, and M. C. Quintero, Spectrochim. Acta, Part B **57,** 1665 (2002).
7. K. Tatekura, Appl. Opt. **22,** 460 (1983).
8. M. Kalal and K. A. Nugent, Appl. Opt. **27,** 1956 (1988).
9. L. M. Smith, D. R. Keefer, and S. I. Sudharsanan, J. Quant. Spectrosc. Radiat. Trans. **39,** 367 (1988).
10. J. Dong and R. J. Kearney, J. Quant. Spectrosc. Radiat. Trans. **46,** 141 (1991).
11. S. Ma, H. Gao, and L. Wu, Appl. Opt. **47,** 1350 (2008).
12. J. Glasser, J. Chapelle, and J. C. Boettner, Appl. Opt. **17,** 3750 (1978).
13. Y. E. Voskoboinikov and N. G. Preobrazhenskii, Opt. Spectrosc. **60,** 111 (1986).
14. M. Deutsch and I. Beniaminy, J. Appl. Phys. **54,** 137 (1983).
15. A. Sáinz, A. Díaz, D. Casas, M. Pineda, F. Cubillo, and M. D. Calzada, Appl. Spectrosc. **60,** 229 (2006).
16. G. N. Minerbo and M. E. Levy, SIAM J. Numer. Anal. **6,** 598 (1969).
17. X.-F. Li, L. Huang, and Y. Huang, J. Phys. A: Math. Theor. **40,** 347 (2006).
18. S. Ma, H. Gao, G. Zhang, and L. Wu, J. Quant. Spectrosc. Radiat. Trans. **107,** 61 (2007).
19. C. J. Cremers and R. C. Birkebak, Appl. Opt. **5,** 1057 (1966).
20. S. A. Yousefi, Appl. Math. Comput. **175,** 574 (2006).
21. G. E. Andrews, R. Askey, and R. Roy, *Special Functions* (Cambridge University Press, Cambridge, 1999).
22. M. J. Buie, J. T. P. Pender, J. P. Holloway, T. Vincent, P. L. G. Ventzek, and M. L. Brake, J. Quant. Spectrosc. Radiat. Trans. **55,** 231 (1996).
23. G. C.-Y. Chan and G. M. Hieftje, Spectrochim. Acta, Part B **61,** 31 (2006).
24. R. S. Anderssen, J. Inst. Math. Appl. **17,** 329 (1976).